Applied Catalysis B: Environmental 300 (2022) 120756

Contents lists available at ScienceDirect

Applied Catalysis B: Environmental

journal homepage: www.elsevier.com/locate/apcatb

Low-crystalline PdCu alloy on large-area ultrathin 2D carbon nitride nanosheets for efficient photocatalytic Suzuki coupling

Xiaoxia Jia [a,1], Jiwu Zhao [c,1], Yujing Lv [a], Xianliang Fu [b], Yajun Jian [a], Weiqiang Zhang [a], Yanyan Wang [a], Huaming Sun [a], Xuxu Wang [c], Jinlin Long [c], Peng Yang [a,*], Quan Gu [a,*], Ziwei Gao [a,*]

[a] Key Laboratory of Applied Surface and Colloid Chemistry, Ministry of Education, Xi'an Key Laboratory of Organometallic Material Chemistry, School of Chemistry and Chemical Engineering, Shaanxi Normal University, Xi'an 710062, China
[b] College of Chemistry and Material Science, Huaibei Normal University, Huaibei, Anhui 235000, China
[c] State Key Laboratory of Photocatalysis on Energy and Environment, Fuzhou University, Fuzhou 350002, China

ARTICLE INFO

Keywords:
Photocatalysis
PdCu alloy
2D ultrathin nanosheets
Carbon nitride
Suzuki cross-coupling

ABSTRACT

We develop a new PdCu/UTCN hybrid by loading low-crystalline PdCu NPs on large-area ultrathin 2D carbon nitride (UTCN) nanosheets that exfoliated from bulk g-C_3N_4 using a twice thermal exfoliation and repolymerization method for photocatalytic Suzuki C-C cross coupling reaction. Due to the advantages of 2D structure of the UTCN and the changes in electronic structure and surface structure of low-crystalline PdCu NPs, PdCu/UTCN shows promoted photocatalytic activity with high selectivity for Suzuki coupling reaction. The TOF value for coupling of iodobenzene with phenylboronic acid is 418.2 h^{-1}, which is 8 and 6.2 times higher than that of previously reported Pd-g-C_3N_4 and Pd based alloy photocatalysts under the same reaction, respectively. Morevoer, this photocatalyst shows a good functional group tolerance as well as good to excellent yield and selectivity for various substrates. This study reports for the first time the PdCu alloy supported UTCN photocatalytic material for enhanced Suzuki reaction.

1. Introduction

Transition metal catalyzed cross-coupling reaction is an effective way to construct C-C and C-X (X is heteroatom) [1–4]. Generally, the transition metal complexes catalyzed homogeneous reaction system (such as Pd complexes) has attracted much attention. The problems of separation and recovery of homogeneous catalysts, use of toxic ligands (PPh_3), and high energy consumption greatly limit their large-scale application (especially for noble metal complex catalysts). It is a very desirable green way to realize C-C coupling reaction by a heterogeneous catalytic system using solar energy instead of heat energy, which has been interested by scientists in the field of photocatalysis and organic synthesis in recent years [5–11]. Pd modified graphitic carbon nitride (g-C_3N_4) hybrid, combining the advantages of g-C_3N_4 [12–15] and Pd active metal, can be considered to be a promising photocatalyst for Suzuki coupling reaction. However, it has faced a grand challenge in terms of reaction activity, selectivity, and the large use of noble metal Pd with the high-cost and toxicity. (1) the separation and migration efficiency of photogenerated charge carriers of bulk g-C_3N_4 is low and perfect Pd nanoparticles (NPs) have low catalytic activity (only some surface atoms are used to activate the substrates), limiting the activtiy and atomic economy. (2) side reactions such as the homo-coupling reaction and redox reaction of substrates simultaneously take place on Pd NPs, lowering the reaction selectivity. Developing integrated structure modulation of hybrid is of great interest in visible light-driven photocatalysis.

In recent years, studies have shown that two-dimensional (2D) nanosheets composed of few atomic layers have attracted extensive attention due to their unique properties and potential applications [16,17]. As a photocatalyst, 2D nanosheet has presented significant advantages including short vertical migration distance of charge carriers from the bulk to the surface, accelerated electron transport along the plane, reduced carrier loss at the material boundary or interface, and large specific surface area for providing abundant reactive sites [18–23].

* Corresponding authors.
E-mail addresses: yangpeng@snnu.edu.cn (P. Yang), guquan@snnu.edu.cn (Q. Gu), zwgao@snnu.edu.cn (Z. Gao).
[1] These authors contributed equally to this work.

https://doi.org/10.1016/j.apcatb.2021.120756
Received 10 June 2021; Received in revised form 28 August 2021; Accepted 24 September 2021
Available online 27 September 2021

Therefore, the development of 2D g-C_3N_4 materials can break through the limitation of photocatalytic properties of bulk materials and several methods have been developed to prepare 2D g-C_3N_4 including liquid exfoliation [20,21,24], thermal etching [19] and so on. However, a facile preparation of large-area ultrathin 2D carbon nitride (UTCN) nanosheets composed of 1–4 atomic layers is still a challenge.

To solve the problems of activity, selectivity, high-cost and toxicity of Pd, proper modifications of the surface supported Pd metals and interface engineering are required to allow effective transfers of photogenerated charge carriers to substances and to adjust catalytic ability of surface metals. Alloying strategy is one of the effective ways, which can not only reduce the amount of used Pd but also further improve the photocatalytic activity and selectivity [25,26]. The reasons for selecting Cu in alloys are that Cu is earth-abundant and low-cost and it as an active metal can activate the halogenated hydrocarbons [27,28]. More importantly, the alloying strategy can change the surface structure and electronic structure of Pd catalytic sites, which can adjust the metal/-semiconductor interface interaction and catalytic activity of metals. For example, alloying can change the crystallinity of primary metal crystals and provide various local atomic arrangements to manipulate the adsorption configuration of reaction substrates. Alloying causes the shift in Fermi level of metals, which leads to changed Schottky barrier at metal/UTCN interface and the promoted photoexcitation process of metals. Moreover, the composition of the alloy is the key to adjust the d-band center of active metals [29,30]. Although alloying strategy (alloying with Au etc.) has been used to improve the efficiency of C-C cross-coupling reactions [7,25,26,31,32], the semiconductor supported PdCu alloy photocatalyst for enhanced photocatalytic Suzuki reaction has not been reported to date.

Herein, we report a novel PdCu alloy NPs modified carbon nitride (PdCu/UTCN) hybrid prepared by loading low-crystalline PdCu alloy NPs on micron-scale ultrathin 2D carbon nitride nanosheets (UTCN) with a thickness of ≈ 1 nm (about 3 layers of C-N) for efficient visible light promoted Suzuki coupling reaction. UTCN has a large specific surface area with S_{BET}= 155.4 m^2/g and a higher separation efficiency of photogenerated electrons and holes. The alloying with Cu promotes the photoexcitation process of metals, adjusts the metal/semiconductor interface interaction for the facilitated transfer of photogenerated electrons from UTCN to metal, and affacts the adsorption and activation of aryl halides and desorption of coupling products. Moreover, low crystallinity of PdCu alloy promotes the adsorption of the product that originated from phenylboronic acid pinacol ester after deboronation by photocatalytic oxidation, facilitating the transmetallation process. As a result, the PdCu/UTCN hybrid shows efficient catalyzed Suzuki coupling reaction at room temperature and further significantly promoted performance with excellent selectivity by visible light irradiation. This material as a solid photocatalyst shows broad functional group tolerance and stability. This work offers a integrated structure modulation strategy to boosting the efficency and selectivity in photocatalytic Suzuki C-C cross-coupling over Pd modified g-C_3N_4 hybrid.

2. Experimental section

2.1. Synthesis of large-area ultrathin 2D carbon nitride (UTCN)

A bulk g-C_3N_4 (BCN) material was prepared by a thermal polymerization method. Melamine (4 g) was mixed and ground with NH_4Cl (10 g) and the mixture was placed in a crucible and annealed at 550 °C for 4 h with a heating rate of 4 °C min^{-1} under an air atmosphere in a muffle furnace. Large-area ultrathin 2D carbon nitride (UTCN) was obtained via a twice thermal exfoliation and repolymerization method. BCN (1 g) in a crucible was annealed at 520 °C for 2 h with a heating rate of 5 °C min^{-1} under an air atmosphere in a muffle furnace to obtained exfoliated sample (thin 2D carbon nitride, TCN). Finally, the UTCN was obtained by a secondary thermal exfoliation and simultaneous polymerization of the TCN at 560 °C for 2 h with a heating rate of 5 °C min^{-1} under an air atmosphere in a muffle furnace.

2.2. Synthesis of PdCu alloy nanoparticles

In a typical synthesis of PdCu alloy nanoparticles (NPs), 0.30 mmol of copper (II) acetylacetonate ($Cu(acac)_2$) and 0.30 mmol of palladium (II) acetylacetonate ($Pd(acac)_2$) were dissolved in 3 mL of oleylamine. The solution was then injected into a mixture of borane-morpholine complex (1.5 mmol), oleylamine (3 mL), and 1-octadecene (7 mL) at 80 °C in Ar atmosphere. The resulting mixture was subsequently raised to 100 °C and kept at this temperature for 1 h. Finally, the product was collected via centrifugation at 9000 rpm for 12 min, washed with a mixture of acetone and ethanol for two times, and it was stored in 30 mL hexane (0.01 mol Pd L^{-1}). A series of Pd_xCu_y alloy NPs with different atomic ratio of Pd and Cu were synthesized under otherwise identical conditions with different ratio of Pd and Cu precursors (0.45 mmol of Pd $(acac)_2$ and 0.15 mmol of $Cu(acac)_2$ for Pd_3Cu_1 alloy NPs; 0.4 mmol of $Pd(acac)_2$ and 0.2 mmol of $Cu(acac)_2$ for Pd_2Cu_1 alloy NPs; 0.2 mmol of $Pd(acac)_2$ and 0.4 mmol of $Cu(acac)_2$ for Pd_1Cu_2 alloy NPs; 0.15 mmol of $Pd(acac)_2$ and 0.45 mmol of $Cu(acac)_2$ for Pd_1Cu_3 alloy NPs). Additionally, monometallic Pd NPs and Cu NPs were also prepared using Cu $(acac)_2$ and $Pd(acac)_2$ alone as precursor through the same protocol.

2.3. Preparation of PdCu/UTCN

PdCu/UTCN hybrid was synthesized by using a self-assembly method. In a typical procedure, 100 mg of UTCN was dispersed in 20 mL hexane and then a certain volume of PdCu alloy NPs solution was added into the UTCN suspension under vigorous stirring for 1.5 h. The final product was obtained by centrifugation and washed with deionized water, followed by drying at 60 °C under air. Pd/UTCN, Cu/UTCN, Pd_xCu_y/UTCN, PdCu/BCN, and PdCu/TCN hybrids were also synthesized via the same method. A series of samples (PdCu/UTCN-x, x = 0.5, 1.5, 2.5, 5, 10, 12.5, 15 mL, represents volume of PdCu alloy NPs solution) with different amount of PdCu were synthesized by changing adding amount of PdCu alloy NPs solution.

2.4. Characterization

The X-Ray Diffraction (XRD) patterns of all samples were collected on Rigaku D/Max2550VB+ /PC (Cu Kα source) at a scan rate of 2.4° min^{-1}. Scanning Electron Microscopy (SEM) images were obtained on a HITACHI SU8220 microscope at an acceleration voltage of 5 kV. Transmission Electron Microscopy (TEM) images and element mapping were obtained by a Tecnai G2 F20 transmission electron microscopy (FEI, USA) at an accelerating voltage of 200 kV. The Aberration-Corrected High-Angle Annular Dark-Field Scanning TEM (HAADF-STEM) and Energy-Dispersive X-Ray Spectroscopy (EDS) mapping were acquired on JEOL-ARM200F transmission electron microscopy. UV–vis absorption spectra were measured by a UV/vis spectrophotometer (UV-Lambda 950, Perkin Elmer). Fourier Transform Infrared (FTIR) spectra were derived from Perkin Elmer Fourier transform infrared spectrometer GX. Photoluminescence (PL) spectra were accomplished in solid with Shimadzu RF5301 Spectrofluorophotometer with an excitation wavelength of 380 nm. Time-Resolved Photoluminescence (TRPL) decay measurements were carried out on a time-correlated single photon counting (TCSPC) Edinburgh FLS 920 fluorescence spectrometer. X-Ray Photoelectron Spectroscopy (XPS) spectra were determined on a VG ESCALAB 250 XPS system with a monochromatized Al Kα X-ray source (15 kV, 200 W). Nitrogen adsorption-desorption isotherms were performed at 77 K using Micromeritics ASAP 2010 equipment. ^1H and ^{13}C Nuclear Magnetic Resonance (NMR) spectra were recorded on a Bruker Avance-600 (600 MHz for 1 H; 151 MHz for 13 C) spectrometer in $CDCl_3$ or DMSO-d_6. For 1 H NMR, tetramethylsilane (TMS) served as internal standard (δ = 0) and 1 H NMR chemical shifts are reported in ppm downfield of tetramethylsilane and referenced to residual solvent peak

($CDCl_3$ at 7.26 ppm, DMSO-d_6 at 2.50 ppm) unless otherwise noted. For ^{13}C NMR, residual solvent was used as internal standard ($CDCl_3$ at 77.00 ppm, DMSO-d_6 at 39.53 ppm) and spectra were obtained with complete proton decoupling. The photoelectrochemical tests were carried out by using the conventional three-electrode electrochemical cell including a working electrode, a platinum wire counter electrode, and an Ag/AgCl reference electrode. The prepared photoelectrodes were used as the working electrode and irradiated under visible light in Na_2SO_4 solution (0.5 M). The X-Ray Absorption Fine Structure (XAFS) spectra were collected at BL14W beamline in Shanghai Synchrotron Radiation Facility (SSRF). The storage ring of SSRF was operated at 3.5 GeV with a stable current of 200 mA. Using Si (111) double-crystal monochromator, the data collection was carried out in fluorescence mode using Lytle detector. All spectra were collected in ambient conditions.

2.5. DFT calculation method

The density function theory (DFT) calculations were performed using Vienna Ab-initio simulation package (VASP) code. According to the experiment fact, 3 atomic layered Pd and PdCu models containing 96 atoms were established and the (111) was exposed, in which the top monolayer of atoms are relaxed during the calculation and the other atoms are fixed to simulate the bulk phase. Similarly, for comparison, an amorphous PdCu cluster containing 10 atoms also was established. In

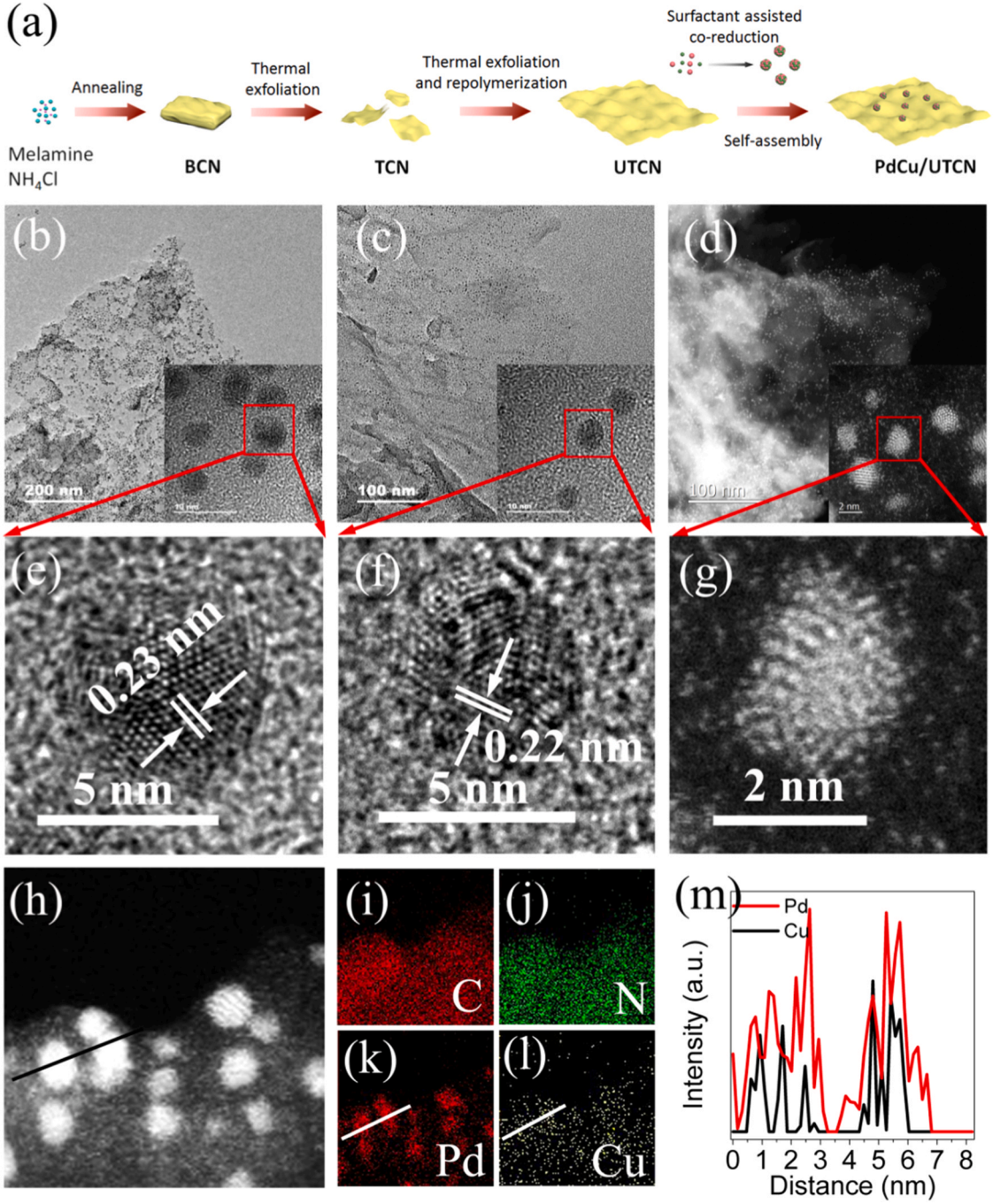

Fig. 1. Schematical illustration of synthesis strategy of PdCu/UTCN (a). TEM and HRTEM images of Pd/UTCN (b and e), and PdCu/UTCN (c and f). HAADF-STEM and atomic-resolution HAADF-STEM images of PdCu/UTCN (d and g). HAADF-STEM image (h) of selected PdCu/UTCN for EELS mapping, 2D EELS map of C, N, Pd, and Cu (i-l) and line distribution of Pd and Cu of PdCu NPs on UTCN (m).

addition, a 20 Å thick vacuum layer was introduced to prevent the interaction between two adjacent slabs. The exchange-correlation function was utilized by generalized gradient approximation-Perdew-Burke-Ernzerhof (GGA-PBE) method. The interaction between core and electron was described by the Projector Augmented Wave (PAW) method, and the cutoff energy was set to 450 eV. The Brillouin-zone integration was performed on 2 × 3 × 2 k points of gamma center for the all calculations. It can be considered that it reached the accuracy require of geometry optimization when force of each atom was less than 0.02 eV/Å.

2.6. Photocatalytic activity measurement

A photocatalytic activity test for Suzuki C-C coupling reaction was carried out in a quartz reactor under visible light irradiation at room temperature. Typically, 50 mg photocatalyst was dispersed in a mixed solution of 4 mL ethanol and 2 mL deionized water, followed by addition of iodobenzene (1.0 mmol), phenylboronic acid pinacol ester (1.5 mmol), and K_2CO_3 (3 mmol) in the reactor. The above suspension was degassed with Ar for 15 min under vigorous stirring to remove air prior to light irradiation. A 300 W Xe lamp (PLS-SXE300UV, Perfectlight) coupled with a cut-off filter ($\lambda \geq 420$ nm) was adopted as the visible light source (the light intensity is 1.0 W cm^{-2}). After the reaction for a certain period of time, the product and unreacted starting substrate were separated by filtration and rotary evaporation. Then, the yield of the product was quantified by gas chromatography (Agilent 7890 A). The turnover frequency (TOF) was calculated from the yield at 10 min based on total Pd amount. The reactions were accomplished at 25 °C.

3. Results and discussion

3.1. Characterizations of PdCu/UTCN photocatalyst

The design strategy of preparation of PdCu/UTCN hybrid is schematically illustrated in Fig. 1a. Large area ultrathin 2D carbon nitride (UTCN) nanosheets was exfoliated from bulk g-C_3N_4 (BCN) using a twice thermal exfoliation and repolymerization method and low-crystalline PdCu NPs were prepared by a surfactant assisted co-reduction method at lower temperature, in which the atomic ratios of Pd to Cu can be controlled by adjusting the concentration of Pd and Cu precursors. Then, the low-crystalline PdCu NPs were well-dispersed on the UTCN by a liquid self-assembly.

We have confirmed the successful preparation of an ultrathin layer of UTCN nanosheets (Figs. S1 and S2) and low-crystalline PdCu NPs alloy (Figs. S3–S5). The UTCN appears a laminar morphology with a thickness of ≈ 1 nm (3 layers of C-N) like silk veil, similar to graphene and the size of the nanosheets reaches micron scale and (Fig. S1c, S1f and S1i), which is in stark contrast from that of BCN (typical monolith like morphology with a thickness of ≈32 nm, Fig. S1a, S1d, and S1g) and TCN (sheet-like with a thickness of ≈6.1 nm, Fig. S1b, S1e, and S1h). PdCu NPs (mean size of 4.68 nm) are uniform and monodisperse (Figs. S3 and S5). HRTEM images show that PdCu NPs present a disordered lattice fringe with a spacing of 2.2 Å assigned to the (111) planes of fcc PdCu alloys (Fig. S3f), whereas Pd NPs have a perfect lattice fringe with a spacing of 2.3 Å for the (111) plane of metallic Pd (Fig. S3e), suggesting that the incorporation of Cu atoms into Pd lattice reduces both the lattice constant and the crystallinity of PdCu NPs.

After loading PdCu alloy on UTCN, the obtained PdCu/UTCN composites were characterized in details. PdCu deposition does not change the microstructure and morphology of UTCN (Fig. 1 and S3-S6). In XRD pattern of the PdCu/UTCN composites (Fig. S3b), a shifted diffraction peak related to the (111) plane of PdCu is very weak and its intensity is not increased even though PdCu amount is increased to 22.5% of theoretical value (Fig. S4c). The shift of peaks and the decrease in intensity can be also observed in Pd_xCu_y/UTCN composites with different Cu/Pd ratio (Fig. S4d), similar to that of unsupported Pd and Pd_xCu_y alloy NPs (Fig. S4a). TEM (Fig. 1c) and aberration-corrected high-angle annular dark-field scanning TEM (HAADF-STEM, Fig. 1d) of the PdCu/UTCN confirm that PdCu NPs with very small size (~2.41 nm, smaller than that of Pd NPs, as shown in Fig. S5) are uniformly dispersed on the UTCN. It is important that the deposition does not change the crystallinity of PdCu alloy, proved by the HRTEM and atomic-resolution HAADF-STEM results show that PdCu NPs on UTCN present a disordered lattice fringe but Pd NPs have a perfect lattice fringe (Fig. 1e-g). Moreover, PdCu NPs intimately contact with UTCN, suggesting the formation of phase junction between PdCu NPs and UTCN (Fig. 1f and g). We also have collected energy-dispersive X-ray spectroscopy (EDS) (Fig. S7) and EDS map scans (Fig. 1i-l) on the selected area in the HAADF-STEM image (Fig. 1h) of the PdCu/UTCN and a line distribution of Cu and Pd of PdCu NPs on UTCN (Fig. 1m). As revealed, Pd and Cu elements are nearly distributed at the same location, suggesting the alloy formation (also be confirmed by Fig. S8).

X-ray photoelectron spectroscopy (XPS) and X-ray absorption fine structure (XAFS) analysis were carried out to investigate chemical state of Pd and Cu of samples. Clearly, the C 1 s and N 1 s peaks attributed to g-C_3N_4 [12,13,33] for Pd/UTCN and PdCu/UTCN shift to the higher binding energy as compared to UTCN (Fig. S9), confirming the interfacial interaction of UTCN with Pd or PdCu NPs. The shift for PdCu/UTCN is less than that for Pd/UTCN, which can be attributed to the electronic interaction between Pd and Cu. In the high resolution Pd 3d XPS spectrum of PdCu/UTCN (Fig. 2a), two major peaks at 335.6 and 340.9 eV can be attributed to Pd^0, while the shoulders at 337.0 and 342.1 eV are ascribed to Pd(II) [12,13,26,29,34,35]. The Pd K-edge spectrum of PdCu/UTCN (Fig. 2c) shows slightly shifted absorption edge and the reduced amplitude as compared to that of Pd foil, but is distinctly different from that of PdO, confirming that Pd in the PdCu/UTCN mainly presents in the metallic state and are slightly oxidized. Consistently, a Pd-O backscattering peak (1.50 Å) and a Pd-Pd backscattering (2.44 Å) peak were observed on k^3-weighted Fourier transform Pd K-edge EXAFS spectrum of PdCu/UTCN (Fig. 2e). Interestingly, the binding energy of Pd 3d for PdCu/UTCN shows a slight shift to higher binding energy with Cu alloying, as compared with that for Pd/UTCN, suggesting the charge transfer between Cu and Pd atoms. The strong peaks centered at 932.4 eV and 952.2 eV for Cu $2p_{3/2}$ and Cu $2p_{1/2}$ in the high-resolution Cu 2p spectrum of PdCu/UTCN (Fig. 2b) and a main peak centered at 918.0 eV in the Cu LMM Auger spectrum (insert of Fig. 2b) indicate that Cu in the PdCu/UTCN mainly presents in the metallic state [26,36,37]. The shoulders located at 933.9 eV and 954.6 eV and satellite peaks located at 943.3 eV and 962.4 eV originate from the surface oxidized Cu [34,36,37]. The extent of oxidized Cu depends on the exposure time of the sample in the air and longtime exposure to air will lead to more surface Cu oxidation. The Cu K-edge spectrum of PdCu/UTCN (the sample for XAFS test was exposed to air for a longer time) shows distinct difference from that of Cu_2O, which further confirming no Cu_2O in the sample. The change in shoulder peak and shift in absorption edge of Cu K-edge indicate that a part of the surface Cu atoms are oxidized to CuO (Fig. 2d). This is consistent with the results reported in the reference [30], which shows that Cu in PdCu alloy is more easily oxidized when the content of Cu is higher. Nevertheless, there is still a small part of Cu in the metallic state. Consistently, k^3-weighted Fourier transform Cu K-edge EXAFS spectrum of PdCu/UTCN shows a distinguished Cu-O backscattering peak (1.46 Å) and a weak Cu-Cu backscattering peak (2.13 Å) (Fig. 2f). Moreover, the Pd-Cu bond also appears in the sample (Table S2), suggesting interaction between Pd and Cu in PdCu alloy. It is important that, upon visible light irradiation, the surface oxidized Cu can be reduced to metallic Cu, as evidenced by the XPS result (Fig. 2b). It is believed that, in the actual photocatalytic reaction process, Pd and Cu species exist in the form of PdCu alloy in which Cu and Pd mainly present in the metallic state.

To further study the effect of PdCu loading on the structure of the catalyst, the optical properties of the PdCu/UTCN as well as BCN, TCN, UTCN, Pd/UTCN and PdCu/BCN reference samples were then

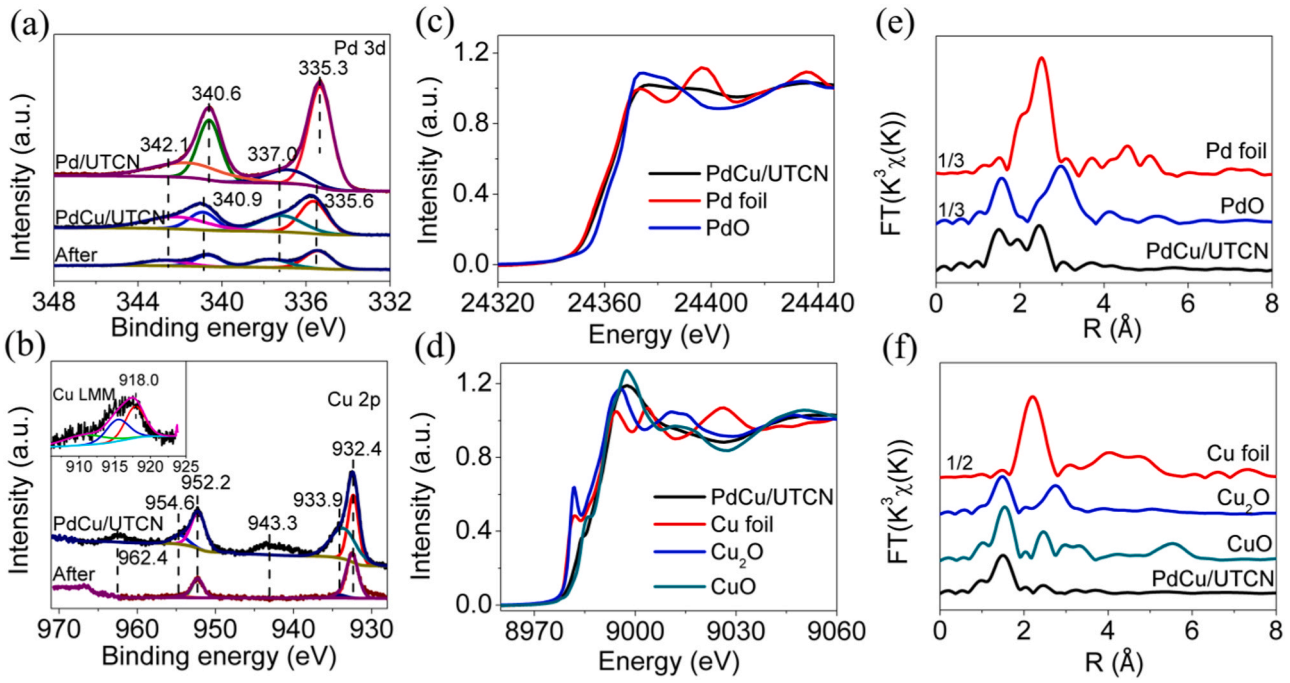

Fig. 2. (a) The high-resolution Pd 3d XPS spectra of Pd/UTCN and PdCu/UTCN before and after light irradiation. (b) The high-resolution Cu 2p XPS spectra of PdCu/UTCN before and after light irradiation, insert of Fig. 2b shows the Cu LMM spectrum of PdCu/UTCN. Normalized (c) Pd K-edge and (d) Cu K-edge XANES spectra of PdCu/UTCN in reference to Pd foil, PdO, Cu foil, Cu_2O, and CuO. k^3-weighted Fourier transform (e) Pd K-edge and (f) Cu K-edge EXAFS spectra.

measured. As shown in UV-Vis DRS spectra (Fig. S1k), UTCN shows a blue shifted absorption edge around at 430 nm in comparison with BCN (463 nm) and TCN (442 nm), which is due to quantum size effect by the exfoliation. Correspondingly, the band-gaps determined from the transformed Kubelka-Munk function decrease from 2.79 eV to 3.04 eV. The absorption edge of Pd/UTCN remains unchanged, but the absorption of visible light from 450 to 800 nm increases significantly. The spectrum of PdCu/UTCN shows a red-shifted absorption edge due to the interaction between UTCN and PdCu NPs and a broad absorption in the visible light region (450–800 nm) caused by PdCu NPs (Fig. S10a) (the similar result is observed for BCN and PdCu/BCN, Fig. S11). Correspondingly, the band-gaps determined from the transformed Kubelka-Munk function decrease from 2.99 eV to 2.86 eV (Fig. S10b). An increase in PdCu NPs loading or the proportion of Cu in PdCu alloy NPs on UTCN leads to a further increased absorption in 450–800 nm (Fig. S11).

3.2. *Photocatalytic Suzuki C-C cross-coupling over PdCu/UTCN*

The photocatalytic performance of the PdCu/UTCN was examined in the Suzuki coupling of aryl halides with phenylboronic acid pinacol ester under visible light irradiation at room temperature. Using the reaction of iodobenzene with phenylboronic acid pinacol ester as the model reaction, the reaction conditions were initially optimized by screening various bases and solvents (Table S5). PdCu/UTCN proved to be a very effective photocatalyst that displays a yield of 96.0% and good recyclability (Fig. 3a and S12f, and Table S6). All PdCu alloy NPs loaded UTCN samples show significant enhanced activity as compared to Pd/UTCN. The yield and initial reaction rate increase with increasing PdCu loading amount due to the increase of active sites, whereas further increasing PdCu loading amount leads to decreased photoactivity, because the enhanced coverage of PdCu NPs on UTCN could block the light absorption of UTCN. At the same loading amount, the photocatalytic activities show a strong correlation with the chemical compositions of the loaded metal NPs (Fig. 3b and S12b). The volcanic relationship between Pd/Cu ratio and photocatalytic activities should be directly related to the active sites. The activity over Pd_xCu_y/UTCN increases with increase of Cu amount and the highest performance is achieved on Pd_1Cu_1/UTCN, which is due to enhanced synergistic effect between Pd and Cu atoms. With the Cu content further increasing, Pd atoms were replaced by a large amount of Cu atoms, which leads to the decrease of Pd active sites. We also found that the performance of the PdCu/UTCN strongly depends on the crystallinity of supported PdCu NPs. As revealed, with increasing of preparation temperature of PdCu NPs, the performance of the samples decreases (Fig. 3b and S12c), suggesting that PdCu NPs with lower crystallinity is more conductive to the photocatalytic Suzuki reaction.

The scope of PdCu/UTCN was explored in the Suzuki coupling reaction of partner substrates, which included aryl, alkenyl and heteroaromatic compounds (Fig. 3c and Table S9). All aryl iodides were converted to the corresponding products in high yields (68.6–96.0%). The steric hindrance of aryl iodides affects the reaction yield (**4** and **5**). The heteroaromatic iodides compound shows low reactivity relative to iodobenzene derivatives (**10**). As a representative for comparison, the turnover frequency (TOF) value of the PdCu/UTCN-2.5 for the coupling of iodobenzene with phenylboronic acid is calculated as high as 418.2 h^{-1}, which is 8 and 6.2 times higher than the highest values of previously reported Pd-g-C_3N_4 (TOF=52 h^{-1}) and Pd based alloy photocatalysts (TOF=68 h^{-1}) in the Suzuki coupling of aryl halides (the same substrates and reaction conditions) (Fig. 3h and Table S11). The desired product of less-reactive aryl bromides can be obtained with yield of 14.7% (**1b**) and corresponding TOF of 2.2 h^{-1}. These values are increased by 2.1 times and 16% as compared to the those of heterogeneous catalytic system using single atom Pd modified carbon nitride catalyst (Pd-ECN) in the same reaction (conversion of 7% and corresponding TOF of 1.9 h^{-1} [38], Table S11). Similarly, using this PdCu/UTCN light promoted protocol, the scope of phenylboronic acid pinacol ester partners was easily extended, allowing installation of aryl groups containing substituents (**11–14**), pyrazole (**15** and **16**) and furan (**17** and **18**) groups. The coupling of C (sp^2) and C (sp^3) can also be realized (**19**) through the photocatalytic Suzuki coupling reactions over our PdCu/UTCN photocatayst. This provides a feasible C(sp^2)-C(sp^3) bond forming protocol for applications in organic synthesis.

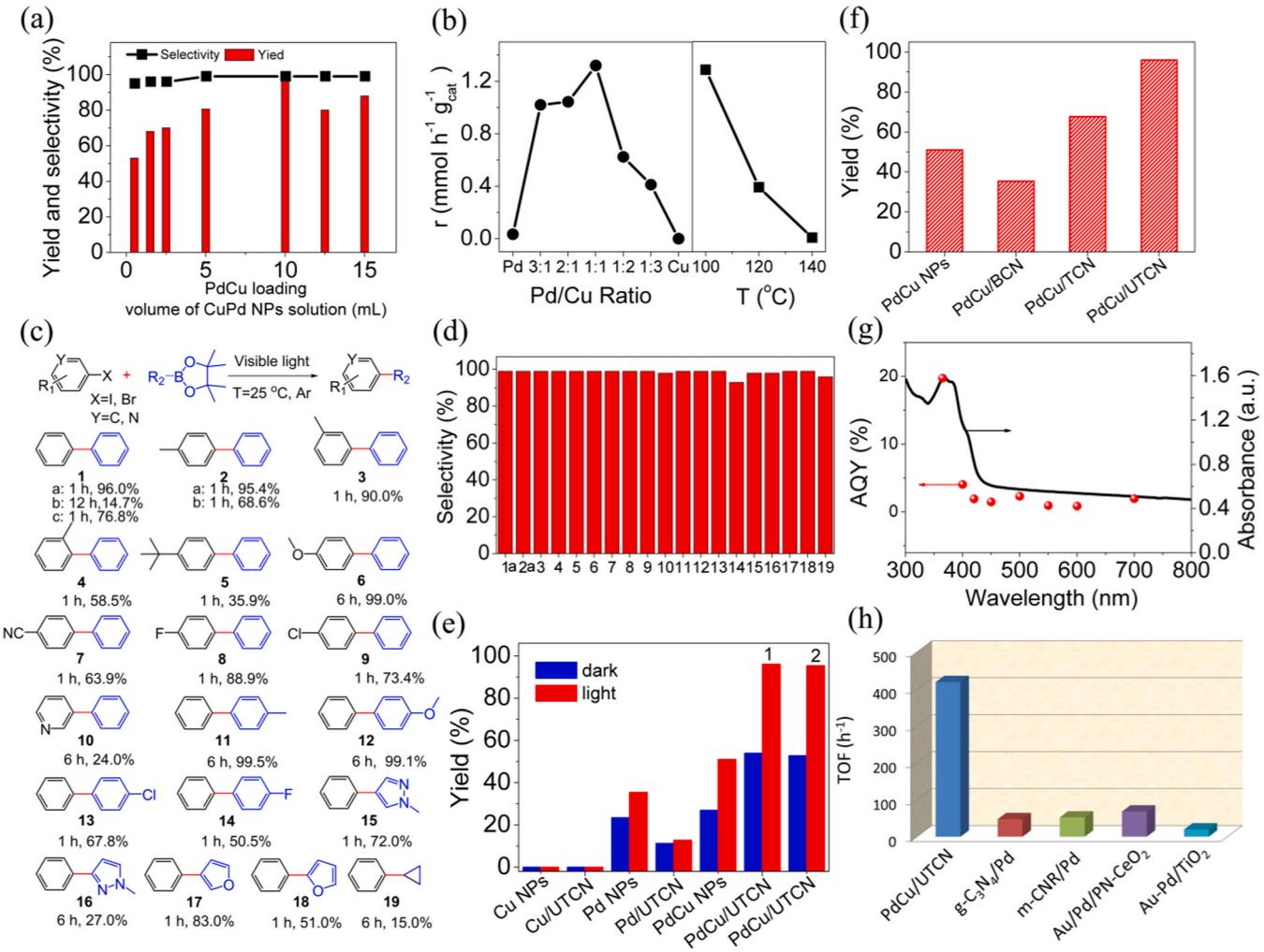

Fig. 3. (a) Effects of PdCu loading on the yield and selectivity of Suzuki reaction of 4-iodotoluene with phenylboronic acid pinacol ester. (b) Effects of Pd/Cu ratio and preparation temperature of PdCu alloy NPs on the initial reaction rate of Suzuki reaction of iodobenzene with phenylboronic acid pinacol ester. (c) Comparative scope of PdCu/UTCN photocatalyst for Suzuki reaction. 1a: coupling of iodobenzene with phenylboronic acid pinacol ester; 1b: coupling of bromobenzene with phenylboronic acid pinacol ester; 1c: coupling of iodobenzene with phenylboronic acid; 2a: coupling of 4-iodotoluene with phenylboronic acid pinacol ester; 2b: coupling of 4-iodotoluene with phenylboronic acid. (d) Selectivity of the desired products (entries 1–19) over PdCu/UTCN. (e) Comparison of Suzuki reaction activity over photocatalysts under dark and visible light irradiation (1 for iodobenzene; 2 for 4-iodotoluene). (f) Comparison of yield of Suzuki C-C coupling over PdCu NPs, PdCu/BCN, PdCu/TCN, and PdCu/UTCN. (g) The AQY values at different wavelengths for biphenyl production calculated from the contribution of light irradiation. (h) Comparison of the turnover frequency reported over g-C_3N_4 based photocatalysts or Pd based alloy photocatalysts in the Suzuki coupling with the same substrates and reaction conditions (coupling of iodobenzene with phenylboronic acid).

What we need to point out is that in addition to the increase of activity, the low-crystalline PdCu alloy also promotes the selectivity of Suzuki reaction. For Pd NPs modified UTCN (Pd/UTCN) samples, the homo-coupling side reaction of aryl halides (such as 4-iodotoluene) substrates simultaneously takes place on Pd NPs to produce 4,4-dimethylbiphenyl, resulting in the low selectivity of cross-coupling product (selectivity of 80%). The homo-coupling process is almost completely inhibited and the cross coupling process is proceeded efficiently on the low crystallinity PdCu alloy NPs loaded UTCN, which makes a excellent selectivity (>99%), as shown in Fig. 3a. Moreover, the PdCu/UTCN photocatalyst shows a excellent selectivity(>93%) for all the above substrates (Fig. 3d). High selectivity of PdCu/UTCN can be attributed to the effect of the surface structure and electronic structure of PdCu alloy on the adsorption and activation of aryl halides and desorption of coupling products, and the promotion of low crystalline structure of PdCu alloy on the transmetallation process, which are described in detail in the following theoretical calculation.

The reactions both in the presence and absence of light at same temperature were tested for comparison (Fig. 3e and Table S7). Pure Cu NPs and Cu/UTCN exhibit no catalytic activity with light irradiation and in the dark. The pure Pd NPs shows a low activity (yield of 23.4%) in the dark and alloying with Cu leads to slightly improved activity (26.3%). Visible light irradiation of both the Pd and PdCu alloy NPs catalysts increases the reaction yield and the enhancement in yield for PdCu NPs is greater than that for Pd NPs. This means that by alloying with Cu enhances the photoinduced performance of Pd NPs. Loading of PdCu alloy on UTCN leads to further enhanced activity, and visible light irradiation of the PdCu/UTCN catalyst significantly increases reaction yield. Obviously, PdCu/UTCN catalyzed Suzuki coupling reaction under light irradiation at room temperature involves the light and thermal processes. For Pd/UTCN (also exhibits light promoted activity), however, it shows decreased performance as compared to pure Pd NPs. These results imply the positive effect of alloying with Cu on the catalytic and photocatalytic activity. No conversion can be observed for the reaction over bare BCN, TCN, and UTCN (Table S7). Similarly, when the PdCu NPs were physically mixed with UTCN nanosheets to catalyze the Suzuki coupling (Table S6, entry 7), the obtained system shows almost the same yield as PdCu NPs, indicating that the proper interfacial

interaction of PdCu NPs with UTCN nanosheets is very important for the photocatalytic Suzuki reactions. For comparison, we also evaluated the Suzuki coupling activity of PdCu/BCN and PdCu/TCN (Fig. 3f and Table S6). The results indicate that the structure of carbon nitride has great effect on the photocatalytic activity in Suzuki coupling reaction.

To better understand the light promoted catalytic performance of PdCu/UTCN, the effect of the intensity and wavelength of incident light on catalytic reaction was investigated. It is found that the yield is almost linear increased with increasing the light intensity (Fig. S14a). The increased light intensity results in the enhanced contribution of light processes to the overall reaction efficiency (increased from 18% at 0.2 W cm^{-2} to 46% at 1.0 W cm^{-2}). As shown in Fig. S14b, the PdCu/UTCN catalyzed Suzuki coupling reaction can be promoted effectively by monochromatic light irradiation in the wavelength range of 365–700 nm compared to the reaction efficiency of the reaction in the dark, but the yields slowly decrease with the increasing wavelength of incident light. The longer the wavelength of incident light, the lower the enhancement that light irradiation produces in the catalytic activity of PdCu/UTCN. As the light absorption threshold of UTCN is 430 nm, the promotion on catalytic activity by light with wavelength greater than 430 nm is attributed to PdCu alloy NPs on UTCN. The variation tendency of AQY curve is coincident with UV–vis DRS spectrum of PdCu/UTCN (Fig. 3g). These results clearly demonstrate the synergistic strengthening effect of UTCN and PdCu alloy on overall light-promoted catalytic activity.

To prove that the light promoted performance comes from the photocatalytic process and to study the roles of photogenerated charge carriers in Suzuki C-C cross-coupling reaction over PdCu/UTCN, carries captured experiments were performed. The results indicate that the p-benzoquinone as an electron scavenger depletes the photogenerated electrons on PdCu NPs (transferred from UTCN and generated by photoexited of PuCu itself), whereas diisopropylethylamine as a hole scavenger blocks hole transfer to the phenylboronic acid pinacol ester, which leads to quenching the reaction (Table S6). These results are consistent with those reported in some literatures [8,31,39,40]. Moreover, the Suzuki reaction was inhibited when it was conducted in oxygen (Table S6) because O_2 molecule as an electron scavenger traps the photogenerated electrons.

3.3. Origin of the superior photocatalytic performance over PdCu/UTCN

Based on the above observations, the light effect is mainly contributed by two processes, including the direct excitation of UTCN producing photogenerated electrons that can migrate to the supported metal and the excitation of PdCu alloy itself by visible light. The significant promotion of light on Suzuki coupling reaction over PdCu/UTCN is attributed to the synergistic effect of 2D structure of UTCN and the alloying of Pd with Cu (Fig. 4).

UTCN has a large specific surface area with S_{BET}= 155.4 m^2/g (higher than that of BCN and TCN (7.8 and 138.6 cm^2/g, respectively), as shwon in Fig. S2 and Table S1). Importantly, compared with BCN and TCN, significant advantages of large-area ultrathin 2D structure of

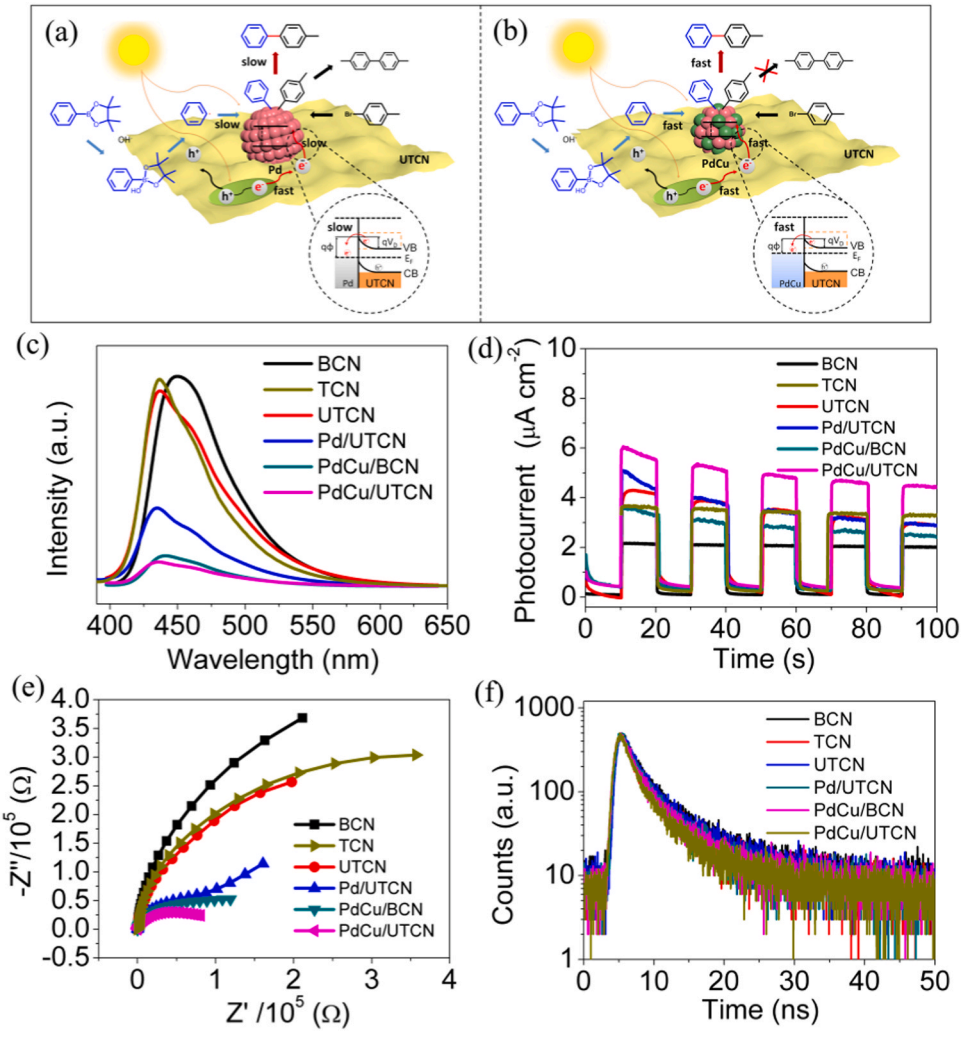

Fig. 4. Schematic illustration of photocatalytic process for the Suzuki cross-coupling reaction and the energy diagrams and processes involving photogenerated charge carriers under illumination of (a) Pd/UTCN and (b) PdCu/UTCN. (c) steady-state PL spectra, (d) electrochemical impedance spectroscopy (EIS) under 1 sun AM 1.5 G simulated solar irradiation, (e) photocurrent (i-t curves) chopping in 0.5 M Na_2SO_4 (pH≈7.0) under 1 sun AM 1.5 G simulated solar irradiation, and (f) time-resolved photoluminescence (TRPL) spectra of BCN, UTCN, Pd/UTCN, PdCu/BCN, and PdCu/UTCN.

UNCN (short vertical migration distance of charge carriers from the bulk to the surface, accelerated electron transport along the plane, reduced carrier loss at the material boundary or interface, and extended π-conjugation system) lead to inhibited charge recombination and the effectively promoted charge separation, which can be proved by the facts that BCN, TCN, and UNCN samples exhibit a progressive decrease in the PL peak (Fig. 4c), a increase in photocurrent density (Fig. 4d), a reduce in charge transfer resistance (Fig. 4e), and a increase in photocatalytic H_2 generation activities (Fig. S11).

Alloying Pd with Cu has a great effect on the separation and migration of photogenerated charge in the photocatalyst. As shown in Fig. 4c, Pd and PdCu NPs loading on UTCN or BCN causes obviouly dereased PL peak and the PdCu/UTCN displays the lowest PL peak attributing to intrinsic excitation. Also, the addition of PdCu alloy NPs to the BCN and UTCN ensues a marked increase to photocurrent denstiy and derease to charge transfer resistance, and the PdCu/UTCN shows the highest photocurrent denstiy and the lowest charge transfer resistance (Fig. 4d and e). The improved stabilization of both electron and hole of PdCu/UTCN can be further confirmed by the time-resolved photoluminescence (TRPL) [41,42], as shown in Fig. 4f. The luminescence decay curves of samples can be fitted and described by two time constants: the radiative process (τ_1) and non-radiative process (τ_2). Thus, the mean lifetimes (τ_m) can be calculated, which are listed in Table S3. The fluorescence lifetimes of PdCu/UTCN are shortest among these samples, which implies that PdCu deposition on UTCN remarkably inhibits the charge recombination. The theoretical calculation results show that the work functions of both Pd and PdCu alloy are larger than that of carbon nitride (Fig. 5a and Table S8) [43]. Both Pd and PdCu alloy can establish valid Schottky junctions with UTCN to improve the electron-hole separation [44,45]. The work function of Pd (Φ_{Pd}=5.20 eV) is larger than that of Cu (Φ_{Cu}=4.51 eV) and the Fermi level of Pd is lower than that of Cu [46,47]. After Pd contacts with Cu to form an alloy, electrons will flow until equilibrium is reached, resulting in higher Fermi level and lower work function of PdCu alloy relative to pure Pd (Fig. S15) [46]. Therefore, the band bending of UTCN formed at PdCu/UTCN interface is smaller than that formed at Pd/UTCN interface [45]. That is to say, the Schottky barrier is reduced (Fig. 5b), which is conducive to the transfer of photogenerated electrons from semiconductor UTCN to metal. We also measured Mott-Schottky curves of UTCN, Pd/UTCN, and PdCu/UTCN to characterize the energy band properties of the photocatalysts and prove the change of the band bending. As shown in Fig. S16, the positive slopes suggest that all of the

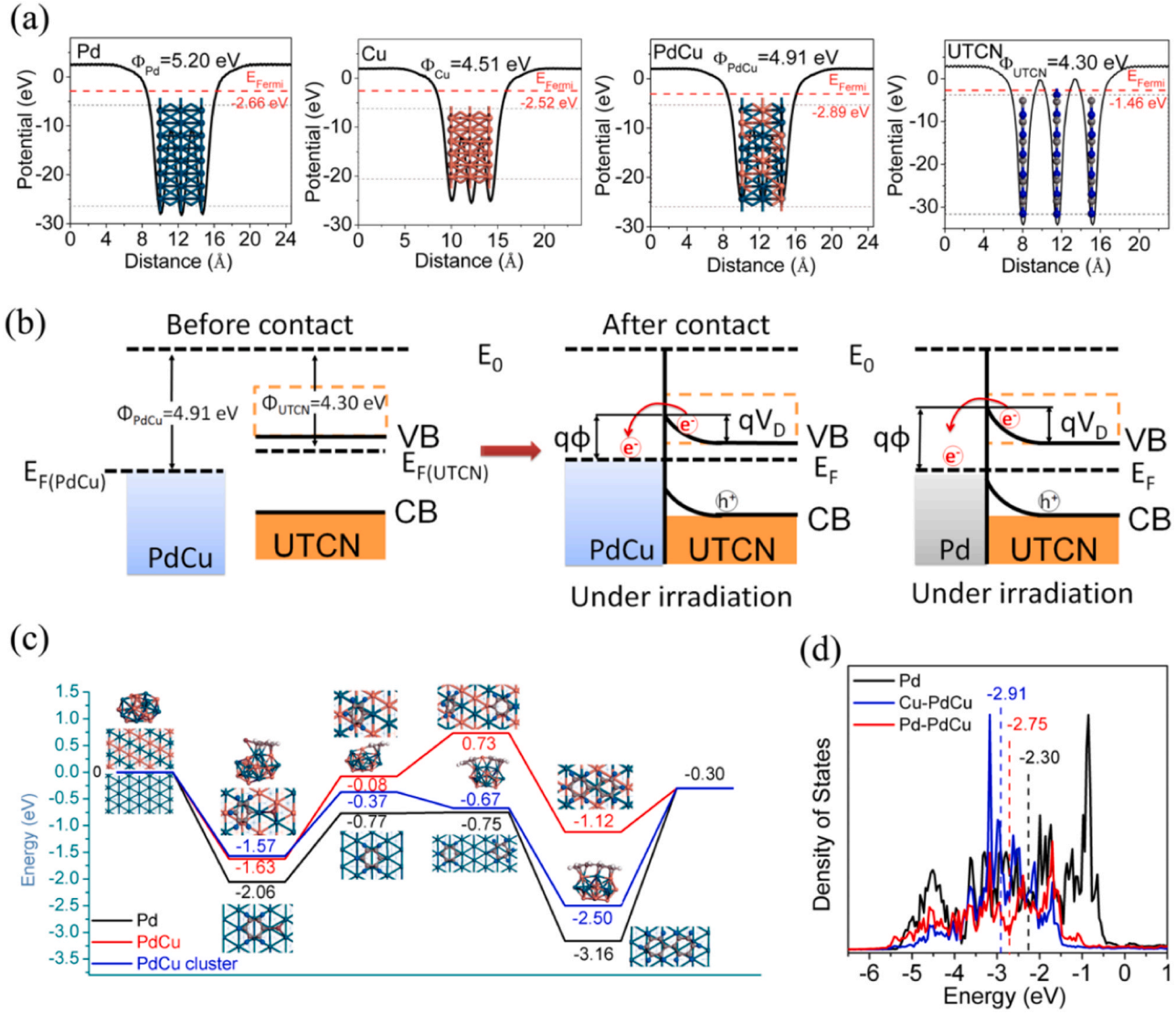

Fig. 5. (a) Work functions of Pd, Cu, PdCu, and UTCN. (b) The formation of Mott-Schottky heterojunctions at PdCu/UTCN and Pd/UTCN interface; (c) Energy profiles of the Suzuki coupling of iodobenzene with phenylboronic acid pinacol ester over Pd, PdCu alloy, and PdCu alloy clusters; (d) Pd d-band center for Pd lattice, and Cu and Pd d-band centers for PdCu lattice.

samples are n-type semiconductors. The flatband potential (E_{fb}) can be obtained from x-intercept of the linear part of the Mott-Schottky plots (Fig. S16). The E_{fb} of UTCN is identified as − 1.14 V vs NHE. The contaction of Pd and PdCu with UTCN leads to the positive shifted E_{fb} for Pd/UTCN and PdCu/UTCN (−0.92 and −1.01 V vs NHE, respectivly) due to the shift of Fermi level and band bending. The positive shift of the E_{fb} of the system means the decrease of the Fermi level of the semiconductor. We can see that, for PdCu/UTCN, the positive shift of E_{fb} is smaller than that of Pd/UTCN, which confirms that alloying Pd with Cu changes Fermi level of metal. These results support the above theoretical analysis. The carrier densities of the samples can be extracted from the slopes of Mott-Schottky plots using equation:

$$N_D = 2/(\varepsilon\varepsilon_0 e) \times (dE/dC^2) = 2/(\varepsilon\varepsilon_0 e)\ (1/slope)$$

where N_D denotes the donor density of the semiconductor, C is the space charge capacitance, ε represents the dielectric constant of g-C_3N_4 (5.25), ε_0 is permittivity in the vacuum level (8.85×10^{-14} F cm^{-1}), e refers to the charge of an electron, and E is applied potential. The calculated carrier density for PdCu/UTCN (1.41×10^{33} cm^{-3}) is found to be higher than that of UTCN (8.09×10^{32} cm^{-3}) and Pd/UTCN (9.17×10^{32} cm^{-3}), confriming the driving and promoting charge transfer by interface junction. Moreover, previous studies have shown that metal Pd can absorb visible light and be excited by LSPR effect and inter band electron transition (the metal Cu has similar properties) [26,32,48–50], and the generated energetic electrons are helpful to the activation of the substrate. The increase of Fermi level after Pd alloying with Cu facilitates the photoexcitation of metals.

In addition to the effect on the charge separation, alloying also affects the surface reaction process, which ultimately affects the activity. We have employed first-principles simulation to search for the reaction path on the surface of pure Pd, perfect PdCu alloy, and PdCu with low crystallinity (Fig. 5c). The PdCu alloy NPs with low crystallinity was approximately replaced by PdCu alloy clusters for convenience of calculation. Upon alloying Pd with Cu and forming lower crystallinity structure, the iodobenzene adsorption on the PdCu surface is relatively weaker than that on Pd surface (the adsorption energy of iodobenzene adsorption decreases from −2.06 eV for pure Pd to −1.57 eV for PdCu alloy clusters), avoiding poisoning and reduced activity of the catalyst. This is because both surface structure (affecting surface energy) and electronic structure (d-band centers) of metals play important roles in the regulating the adsorption of substrates. The surface energy of (111) surface decreases from 1.28 J/m^2 for pure Pd to 0.90 J/m^2 for PdCu alloy. The Pd d-band center of PdCu is lower than that of pure Pd (−2.30 eV versus −2.75 eV) (Fig. 5d). The C-I dissociation process of iodobenzene presents an energy barrier for activation. Although the perfect PdCu alloy has a higher energy barrier as compared to pure Pd (1.55 eV and 1.29 eV for perfect PdCu alloy and pure Pd, respectively), the decreased crystallinity of PdCu alloy reduces this barrier (1.20 eV), suggesting the promoted C-I dissociation of iodobenzene for Suzuki C-C cross coupling reaction. More importantly, the amorphous structure of PdCu alloy promotes the adsorption of the product that originated from phenylboronic acid pinacol ester after deboronation by photocatalytic oxidation, facilitating the transmetallation process. Finally, desorption of the coupling products is also one of the main factors affecting the catalytic activity. Interestingly, the adsorption of biphenyl product on the pure Pd (111) surface is too strong and correspondingly the desorption energy is larger (2.86 eV), whereas PdCu alloy has moderate adsorption energy due to the adjustment of surface energy and desorption energy of biphenyl on perfect PdCu alloy and PdCu alloy clusters surface decreased to be 0.82 eV and 2.2 eV (Fig. 5c), which is conducive to cross-coupling reaction.

4. Conclusions

In conclusion, a new PdCu/UTCN hybrid is constructed by loading low-crystalline PdCu NPs on micron-scale ultrathin 2D carbon nitride (UTCN) nanosheets for photocatalytic Suzuki C-C cross couplng reaction. This PdCu/UTCN composite shows significantly visible light improved catalytic activity with high selectivity for Suzuki coupling reaction as compared with PdCu NPs and Pd/UTCN, which originates from synergistic effect of 2D structure of UTCN and alloying of Pd with Cu. The 2D structure of UTCN provides large specific surface area and allows efficient separation and migration of photogenerated carriers. The low crystalline PdCu NPs can play three roles in activity and selectivity of Suzuki C-C cross coupling reaction: (1) Alloying Pd with Cu causes the increase in Fermi level of PdCu alloy relative to Pd, leading to the reduced Schottky barrier at metal/UTCN interface and also the promoted photoexcitation process of metals. (2) Alloying Pd with Cu affects the adsorption and activation of aryl halides and desorption of coupling products. (3) low crystallinity of PdCu alloy promotes the adsorption of the product that originated from phenylboronic acid pinacol ester after deboronation by photocatalytic oxidation, facilitating the transmetallation process. Moreover, this photocatalyst has broad functional group tolerance and reusability, suggesting that it is obviously more suitable for practical applications.

CRediT authorship contribution statement

Xiaoxia Jia: Investigation, Writing – original draft. **Jiwu Zhao:** Investigation, Methodology, Software. **Yujing Lv:** Validation. **Xianliang Fu:** Data curation, Funding acquisition. **Yajun Jian:** Formal analysis, Data curation. **Weiqiang Zhang:** Formal analysis. **Yanyan Wang:** Formal analysis. **Huaming Sun:** Resources. **Xuxu Wang:** Writing – review & editing. **Jinlin Long:** Resources, Writing – review & editing. **Peng Yang:** Funding acquisition, Writing – review & editing. **Quan Gu:** Conceptualization, Supervision, Writing – original draft, Funding acquisition. **Ziwei Gao:** Supervision.

Declaration of Competing Interest

The authors declare that they have no known competing financial interests or personal relationships that could have appeared to influence the work reported in this paper.

Acknowledgements

This work is financially supported by the National Natural Science Foundation of China (No. 21872089), the Fundamental Research Funds for the Central Universities (No. GK202103025), the Innovation Capability Support Program of Shaanxi (Program No. 2020TD024), the 111 Project (B14041), and Natural Science Foundation of Anhui Province for Distinguished Young Scholars (No. 1808085J24).

Appendix A. Supporting information

Supplementary data associated with this article can be found in the online version at doi:10.1016/j.apcatb.2021.120756.

References

[1] A. Suzuki, Cross-coupling reactions of organoboranes: an easy way to construct C-C bonds (Nobel Lecture), Angew. Chem. Int. Ed. 50 (2011) 6722–6737.
[2] F.S. Han, Transition-metal-catalyzed Suzuki-Miyaura cross-coupling reactions: a remarkable advance from palladium to nickel catalysts, Chem. Soc. Rev. 42 (2013) 5270–5298.
[3] R. Jana, T.P. Pathak, M.S. Sigman, Advances in transition metal (Pd,Ni,Fe)-catalyzed cross-coupling reactions using alkyl-organometallics as reaction partners, Chem. Rev. 111 (2011) 1417–1492.
[4] C.K. Prier, D.A. Rankic, D.W.C. MacMillan, Visible light photoredox catalysis with transition metal complexes: applications in organic synthesis, Chem. Rev. 113 (2013) 5322–5363.
[5] Q. Gu, Q. Jia, J. Long, Z. Gao, Heterogeneous photocatalyzed C−C cross-coupling reactions under visible-light and near-infrared light irradiation, ChemCatChem 11 (2019) 669–683.

[6] F. Raza, D. Yim, J.H. Park, H.I. Kim, S.J. Jeon, J.H. Kim, Structuring Pd nanoparticles on 2H-WS_2 nanosheets induces excellent photocatalytic activity for cross-coupling reactions under visible light, J. Am. Chem. Soc. 139 (2017) 14767–14774.

[7] S. Sarina, H. Zhu, E. Jaatinen, Q. Xiao, H. Liu, J. Jia, C. Chen, J. Zhao, Enhancing catalytic performance of palladium in gold and palladium alloy nanoparticles for organic synthesis reactions through visible light irradiation at ambient temperatures, J. Am. Chem. Soc. 135 (2013) 5793–5801.

[8] Z.J. Wang, S. Ghasimi, K. Landfester, K.A.I. Zhang, Photocatalytic suzuki coupling reaction using conjugated microporous polymer with immobilized palladium nanoparticles under visible light, Chem. Mater. 27 (2015) 1921–1924.

[9] Y. Li, Z. Zhang, L. Pei, X. Li, T. Fan, J. Ji, J. Shen, M. Ye, Multifunctional photocatalytic performances of recyclable Pd-$NiFe_2O_4$/reduced graphene oxide nanocomposites via different co-catalyst strategy, Appl. Catal. B: Environ. 190 (2016) 1–11.

[10] Z. Li, Y. Pi, D. Xu, Y. Li, W. Peng, G. Zhang, F. Zhang, X. Fan, Utilization of MoS_2 and graphene to enhance the photocatalytic activity of Cu_2O for oxidative C-C bond formation, Appl. Catal. B: Environ. 213 (2017) 1–8.

[11] Z. Lou, Q. Gu, Y. Liao, S. Yu, C. Xue, Promoting Pd-catalyzed Suzuki coupling reactions through near-infrared plasmon excitation of WO_{3-x} nanowires, Appl. Catal. B: Environ. 184 (2016) 258–263.

[12] Q. Jia, S. Zhang, Q. Gu, C-C formation mediated by photoinduced electrons from crystallized carbon nitride nanobelts under visible light irradiation, J. Energy Chem. 30 (2019) 152–161.

[13] Q. Jia, S. Zhang, X. Jia, X. Dong, Z. Gao, Q. Gu, Photocatalytic coupled redox cycle for two organic transformations over Pd/carbon nitride composites, Catal. Sci. Technol. 9 (2019) 5077–5089.

[14] X.-H. Li, M. Baar, S. Blechert, M. Antonietti, Facilitating room-temperature Suzuki coupling reaction with light: Mott-Schottky photocatalyst for C-C-coupling, Sci. Rep. 3 (2013) 1–6.

[15] C. Yang, B. Wang, L. Zhang, L. Yin, X. Wang, Synthesis of layered carbonitrides from biotic molecules for photoredox transformations, Angew. Chem. Int. Ed. 56 (2017) 6627–6631.

[16] M. Chhowalla, H.S. Shin, G. Eda, L.-J. Li, K.P. Loh, H. Zhang, The chemistry of two-dimensional layered transition metal dichalcogenide nanosheets, Nat. Chem. 5 (2013) 263–275.

[17] A. Zavabeti, A. Jannat, L. Zhong, A.A. Haidry, Z. Yao, J.Z. Ou, Two-dimensional materials in large-areas: synthesis, properties and applications, Nano-Micro Lett. 12 (2020) 66.

[18] W. Jiang, H. Wang, X. Zhang, Y. Zhu, Y. Xie, Two-dimensional polymeric carbon nitride: structural engineering for optimizing photocatalysis, Sci. China Chem. 61 (2018) 1205–1213.

[19] P. Niu, L. Zhang, G. Liu, H.-M. Cheng, Graphene-like carbon nitride nanosheets for improved photocatalytic activities, Adv. Funct. Mater. 22 (2012) 4763–4770.

[20] H. Ou, L. Lin, Y. Zheng, P. Yang, Y. Fang, X. Wang, Tri-s-triazine-based crystalline carbon nitride nanosheets for an improved hydrogen evolution, Adv. Mater. 29 (2017), 1700008.

[21] S. Yang, Y. Gong, J. Zhang, L. Zhan, L. Ma, Z. Fang, R. Vajtai, X. Wang, P. M. Ajayan, Exfoliated graphitic carbon nitride nanosheets as efficient catalysts for hydrogen evolution under visible light, Adv. Mater. 25 (2013) 2452–2456.

[22] J. Xiong, P. Song, J. Di, H. Li, Ultrathin structured photocatalysts: a versatile platform for CO_2 reduction, Appl. Catal. B: Environ. 256 (2019), 117788.

[23] D. Huang, Z. Li, G. Zeng, C. Zhou, W. Xue, X. Gong, X. Yan, S. Chen, W. Wang, M. Cheng, Megamerger in photocatalytic field: 2D g-C_3N_4 nanosheets serve as support of 0D nanomaterials for improving photocatalytic performance, Appl. Catal. B: Environ. 240 (2019) 153–173.

[24] X. Zhang, X. Xie, H. Wang, J. Zhang, B. Pan, Y. Xie, Enhanced photoresponsive ultrathin graphitic-phase C_3N_4 nanosheets for bioimaging, J. Am. Chem. Soc. 135 (2013) 18–21.

[25] P. Verma, Y. Kuwahara, K. Mori, H. Yamashita, Synthesis and characterization of a Pd/Ag bimetallic nanocatalyst on SBA-15 mesoporous silica as a plasmonic catalyst, J. Mater. Chem. A 3 (2015) 18889–18897.

[26] B. Wang, Y. Wang, J. Li, X. Guo, G. Bai, X. Tong, G. Jin, X. Guo, Photocatalytic Sonogashira reaction over silicon carbide supported Pd–Cu alloy nanoparticles under visible light irradiation, Catal. Sci. Technol. 8 (2018) 3357–3362.

[27] J. Hassan, M. Sévignon, C. Gozzi, E. Schulz, M. Lemaire, Aryl−aryl bond formation one century after the discovery of the Ullmann reaction, Chem. Rev. 102 (2002) 1359–1470.

[28] L. Zhu, G. Li, L. Luo, P. Guo, J. Lan, J. You, Highly functional group tolerance in copper-catalyzed N-arylation of nitrogen-containing heterocycles under mild conditions, J. Org. Chem. 74 (2009) 2200–2202.

[29] X. Cai, A. Wang, J. Wang, R. Wang, S. Zhong, Y. Zhao, L. Wu, J. Chen, S. Bai, Order engineering on the lattice of intermetallic PdCu co-catalysts for boosting the photocatalytic conversion of CO_2 into CH_4, J. Mater. Chem. A 6 (2018) 17444–17456.

[30] R. Long, Y. Li, Y. Liu, S. Chen, X. Zheng, C. Gao, C. He, N. Chen, Z. Qi, L. Song, J. Jiang, J. Zhu, Y. Xiong, Isolation of Cu atoms in Pd lattice: forming highly selective sites for photocatalytic conversion of CO_2 to CH_4, J. Am. Chem. Soc. 139 (2017) 4486–4492.

[31] D. Han, Z. Bao, H. Xing, Y. Yang, Q. Ren, Z. Zhang, Fabrication of plasmonic Au-Pd alloy nanoparticles for photocatalytic Suzuki-Miyaura reactions under ambient conditions, Nanoscale 9 (2017) 6026–6032.

[32] Q. Xiao, S. Sarina, A. Bo, J. Jia, H. Liu, D.P. Arnold, Y. Huang, H. Wu, H. Zhu, Visible light-driven cross-coupling reactions at lower temperatures using a photocatalyst of palladium and gold alloy nanoparticles, ACS Catal. 4 (2014) 1725–1734.

[33] J. Liu, Q. Jia, J. Long, X. Wang, Z. Gao, Q. Gu, Amorphous NiO as co-catalyst for enhanced visible-light-driven hydrogen generation over g-C_3N_4 photocatalyst, Appl. Catal. B: Environ. 222 (2018) 35–43.

[34] J. He, D. Chen, N. Li, Q. Xu, H. Li, J. He, J. Lu, Controlled fabrication of mesoporous ZSM-5 zeolite-supported PdCu alloy nanoparticles for complete oxidation of toluene, Appl. Catal. B: Environ. 265 (2020), 118560.

[35] W. Li, X.-S. Chu, F. Wang, Y.-Y. Dang, X.-Y. Liu, X.-C. Wang, C.-Y. Wang, Enhanced cocatalyst-support interaction and promoted electron transfer of 3D porous g-C_3N_4/GO-M (Au, Pd, Pt) composite catalysts for hydrogen evolution, Appl. Catal. B: Environ. 288 (2021), 120034.

[36] S. Poulston, P.M. Parlett, P. Stone, M. Bowker, Surface oxidation and reduction of CuO and Cu_2O studied using XPS and XAES, Surf. Interface Anal. 24 (1996) 811–820.

[37] J.P. Espinós, J. Morales, A. Barranco, A. Caballero, J.P. Holgado, A.R. González-Elipe, Interface effects for Cu, CuO, and Cu_2O deposited on SiO_2 and ZrO_2. XPS determination of the valence state of copper in Cu/SiO_2 and Cu/ZrO_2 catalysts, J. Phys. Chem. B 106 (2002) 6921–6929.

[38] Z. Chen, E. Vorobyeva, S. Mitchell, E. Fako, M.A. Ortuño, N. López, S.M. Collins, P. A. Midgley, S. Richard, G. Vilé, J. Pérez-Ramírez, A heterogeneous single-atom palladium catalyst surpassing homogeneous systems for Suzuki coupling, Nat. Nanotechnol. 13 (2018) 702–707.

[39] Z. Jiao, Z. Zhai, X. Guo, X.-Y. Guo, Visible-light-driven photocatalytic Suzuki–Miyaura coupling reaction on Mott–Schottky-type Pd/SiC catalyst, J. Phys. Chem. C 119 (2015) 3238–3243.

[40] Y. Luo, Y. Peng, W. Liu, F. Chen, B. Wang, Soluble porous coordination frameworks constructed from inorganic nanoparticles as homogenized heterogeneous photocatalysts for Suzuki coupling reactions under near-infrared light, Chem. - Eur. J. 23 (2017) 8879–8885.

[41] S. Cao, Y. Li, B. Zhu, M. Jaroniec, J. Yu, Facet effect of Pd cocatalyst on photocatalytic CO_2 reduction over g-C_3N_4, J. Catal. 349 (2017) 208–217.

[42] D. Dong, C. Yan, J. Huang, N. Lu, P. Wu, J. Wang, Z. Zhang, An electron-donating strategy to guide the construction of MOF photocatalysts toward co-catalyst-free highly efficient photocatalytic H_2 evolution, J. Mater. Chem. A 7 (2019) 24180–24185.

[43] B. Zhu, J. Zhang, C. Jiang, B. Cheng, J. Yu, First principle investigation of halogen-doped monolayer g-C_3N_4 photocatalyst, Appl. Catal. B: Environ. 207 (2017) 27–34.

[44] X.-H. Li, M. Antonietti, Metal nanoparticles at mesoporous N-doped carbons and carbon nitrides: functional Mott–Schottky heterojunctions for catalysis, Chem. Soc. Rev. 42 (2013) 6593–6604.

[45] Z. Zhang, J.T. Yates, Band bending in semiconductors: chemical and physical consequences at surfaces and interfaces, Chem. Rev. 112 (2012) 5520–5551.

[46] A.D. van Langeveld, H.A.C.M. Hendrickx, B.E. Nieuwenhuys, The surface composition of Pd-Cu alloys: a comparative investigation of photoelectric work function measurements, Auger electron spectroscopy and calculations based on a broken bond approximation, Thin Solid Films 109 (1983) 179–192.

[47] H.L. Skriver, N.M. Rosengaard, Surface energy and work function of elemental metals, Phys. Rev. B 46 (1992) 7157–7168.

[48] T.T. Trinh, R. Sato, M. Sakamoto, Y. Fujiyoshi, M. Haruta, H. Kurata, T. Teranishi, Visible to near-infrared plasmon-enhanced catalytic activity of Pd hexagonal nanoplates for the Suzuki coupling reaction, Nanoscale 7 (2015) 12435–12444.

[49] M. Koohgard, M. Hosseini-Sarvari, Enhancement of Suzuki–Miyaura coupling reaction by photocatalytic palladium nanoparticles anchored to TiO_2 under visible light irradiation, Catal. Commun. 111 (2018) 10–15.

[50] Q. Xiao, S. Sarina, E. Jaatinen, J. Jia, D.P. Arnold, H. Liu, H. Zhu, Efficient photocatalytic Suzuki cross-coupling reactions on Au–Pd alloy nanoparticles under visible light irradiation, Green Chem. 16 (2014) 4272–4285.